
DoubleML_{Deep}: Estimation of Causal Effects with Multimodal Data

Sven Klaassen^{1,2} Jan Teichert-Kluge² Philipp Bach² Victor Chernozhukov³ Martin Spindler^{1,2}
 Suhas Vijaykumar³

Abstract

This paper explores the use of unstructured, multimodal data, namely text and images, in causal inference and treatment effect estimation. We propose a neural network architecture that is adapted to the double machine learning (DML) framework, specifically the partially linear model. An additional contribution of our paper is a new method to generate a semi-synthetic dataset which can be used to evaluate the performance of causal effect estimation in the presence of text and images as confounders. The proposed methods and architectures are evaluated on the semi-synthetic dataset and compared to standard approaches, highlighting the potential benefit of using text and images directly in causal studies. Our findings have implications for researchers and practitioners in economics, marketing, finance, medicine and data science in general who are interested in estimating causal quantities using non-traditional data.

1. Introduction

In this paper, we delve into the realm of causal inference and treatment effect estimation in the presence of high-dimensional and unstructured multimodal confounders, emphasizing the utilization of deep learning techniques for handling complex nuisance parameters. In many cases, text and image data contain information that can otherwise not be accounted for in causal studies, for example in the form of sentiment in product descriptions or reviews, labels for product images in online marketplaces or health information encoded in medical images. In causal studies, this information can be very important to account for otherwise unmeasured confounding or to improve estimation precision of causal effects. Our focus is on developing

methods that ensure root- N consistency and valid inferential statements of the causal parameter, particularly in scenarios where traditional semi-parametric assumptions are challenged by the increasing complexity of the nuisance parameter space (Foster & Syrgkanis, 2023). The parameter of interest will typically be a causal or treatment effect parameter, denoted by θ_0 . Common examples for θ_0 include the average treatment effect (ATE) or the ATE for the subgroup of the Treated (ATT). We consider settings in which the nuisance parameters / functions will be estimated using deep learning methods, such as transformers, or large language models (LLM). These deep learning methods are capable of handling high-dimensional, unstructured covariates, like texts and images (Goodfellow et al., 2016; Zhang et al., 2023), and provide estimators of nuisance functions when these functions are highly complex. In this context, "highly complex" means that the entropy of the parameter space associated with the nuisance parameter increases with the sample size, going beyond the conventional framework addressed in the classical semi-parametric literature (Härdle et al., 2012). The main contribution of this paper is to offer a general procedure for estimation and inference on θ_0 that is formally valid in these highly complex settings. In Section 5.1, we also propose a method to generate semi-synthetic data in the presence of text and images as confounders. Data generating processes for unstructured data are characterized by inherent challenges, which are briefly summarized and addressed in our paper. Given the growing interest in causal inference with text and image data and the increased availability of this data, we believe that this contribution of our paper might be of independent interest.

As a lead example, we consider the following partially linear regression (PLR) model (Chernozhukov et al., 2018):

$$Y = \theta_0 D + g_0(X) + \varepsilon, \quad \mathbb{E}[\varepsilon|X, D] = 0 \quad (1)$$

$$D = m_0(X) + \vartheta, \quad \mathbb{E}[\vartheta|X] = 0 \quad (2)$$

Here, Y is the outcome variable, D is the policy/treatment variable of interest, X consists of other controls, and ε and ϑ are disturbances. The first equation is the main equation, and θ_0 is the main regression coefficient we would like to infer. If D is conditionally exogenous on controls X , θ_0 has the interpretation of the average treatment effect parameter or the "lift" parameter in business applications. The second

^{*}Equal contribution ¹Economic AI GmbH, Germany ²University of Hamburg, Germany ³Massachusetts Institute of Technology, USA. Correspondence to: Sven Klaassen <sven.klaassen@uni-hamburg.de>.

equation keeps track of confounding, namely the dependence of the treatment variable on controls. This equation is not of interest per se but is important for characterizing and removing regularization bias. Confounders X affect the policy variable D through the function $m_0(X)$ and the outcome variable via the function $g_0(X)$. Not correctly accounting for all confounding factors, e.g. by not including all relevant confounders X , may lead to biased estimates of the target parameter θ_0 . In real world applications the confounding factors might be very complex and hard to observe or measure (e.g. product quality or medical information). Text and image data can be helpful to control for these complex confounding factors, for instance product images and descriptions are usually a good indicator of product quality. Consequently, causal models can benefit from text and image data to remove selection bias. We leverage deep learning methods to fit functions representing the conditional expectations of the output variable Y and the treatment variable D given our set of covariates. Specifically, we define:

$$l_0(X) := \mathbb{E}[Y|X] \quad (3)$$

$$m_0(X) := \mathbb{E}[D|X] \quad (4)$$

To construct an orthogonalized score for the fitted nuisance learners $\hat{\eta} = (\hat{l}, \hat{m})$, we define the following expression:

$$\psi(W, \theta, \hat{\eta}) := \left(Y - \hat{l}(X) - \theta (D - \hat{m}(X)) \right) \cdot (D - \hat{m}(X)),$$

where $W = (Y, D, X)$. The construction of an orthogonalized score ensures the necessary orthogonality for valid causal inference. Finally, the estimate is computed as the solution to the following equation:

$$0 = \frac{1}{n} \sum_{i=1}^n \psi(W_i, \hat{\theta}, \hat{\eta}_0)$$

The assumptions involve bounding the difference between estimated nuisance functions (\hat{m} and \hat{l}) and true functions (m_0 and l_0) in relation to the sample size N

$$\begin{aligned} & \|\hat{m}(X) - m_0(X)\|_{P,2} \\ & \cdot \left(\|\hat{m}(X) - m_0(X)\|_{P,2} + \|\hat{l}(X) - l_0(X)\|_{P,2} \right) \quad (5) \\ & \leq \delta_N N^{-1/2}. \end{aligned}$$

Under this assumption and additional regularity conditions¹, the estimator $\hat{\theta}$ converges to the true parameter θ_0 at a rate of $1/\sqrt{n}$ and is approximately normally distributed:

$$\sqrt{n}(\hat{\theta} - \theta_0) \rightarrow \mathcal{N}(0, \sigma^2)$$

¹ δ_N is a sequence of positive constants converging to zero. For details on the regularity conditions, see Chernozhukov et al. (2018).

This methodology forms the basis for treatment effect estimation in the presence of high-dimensional unstructured confounders. In modern research, the availability of unstructured data, such as images and text, has become ubiquitous. These data types offer a rich source of information that can contribute significantly to the estimation of causal effects. Incorporating unstructured data into the causal models such as the PLR as controls introduces several advantages. First, it allows for a more comprehensive representation of the confounding structure, capturing nuances that may be missed by solely relying on structured / tabular covariates. Second, more and more deep learning models are being developed which are tailored for unstructured data, such as transformers for images or LLMs for text, can be seamlessly integrated into the estimation process, further enhancing the accuracy of nuisance parameter estimation (Chernozhukov et al., 2018). Third, we would like to note that we focus specifically on the semi-parametric PLR model in this paper. In general, our methodology is basically also applicable to other nonparametric causal models that share the key ingredients of the double machine learning framework (cf. Section 3).

In the subsequent sections, we elaborate on the methodology for leveraging unstructured data within the PLR framework and present simulation studies based on the semi-synthetic dataset.

2. Literature Review and Examples

The use of unstructured data such as images and text as controls is crucial for identification and estimation of causal parameters, for example for estimating price elasticities, effects of medical treatments (Chan et al., 2018; Masukawa et al., 2022), or the effect of condensation trails on the climate (Wu et al., 2023). While unstructured data have been used for prediction tasks for some time, e.g. deep learning techniques for clinical risk predictions (Zhang et al., 2020), the use of text and images for causal inference has been a very recent development in the scientific literature. Text as outcome and treatment variable was discussed in Egami et al. (2018) and Sridhar & Blei (2022), but on a very high / conceptual level. We focus on text (and images) as confounders. Veitch et al. (2020) consider this setting and provide results for the consistency of the causal estimate, while we integrate it into the double machine learning framework to perform valid inference, i.e. constructing valid confidence intervals and test statistics for causal parameters. Melnychuk et al. (2022) apply transformer to estimate treatment effects with tabular data and time-varying covariates, but also not provide inference results. The recent literature on the use of text for causal inference is nicely summarized in Feder et al. (2022). There are also approaches to use images in causal inference

(Jerzak et al., 2023a;b;c), but we are, to the best of our knowledge, not aware of any study allowing for valid inference with images and consider our approach as the first to integrate both text and images in a *multimodal* double machine learning framework.

3. Getting started / Warm up: Double Machine Learning for Tabular Data

The double machine learning method, as proposed by Chernozhukov et al. (2018), is a framework that aims to provide valid statistical inference in structural equation models while leveraging the predictive power of machine learning methods for potentially high-dimensional and non-linear nuisance functions. The DML framework consists of three key ingredients:

- Neyman orthogonality
- High-quality machine learning estimation
- Sample splitting

Neyman orthogonality ensures that the score function $\psi(W, \theta, \hat{\eta})$ to estimate the target parameter θ_0 is insensitive towards the plug-in estimates from the nuisance learners $\hat{\eta}$. This is specifically relevant for machine learning algorithms such as neural networks, as these usually trade off variance and bias to achieve high-quality predictions via regularization.

High-quality machine learning estimation involves using state-of-the-art machine learning algorithms to estimate the nuisance functions in Equations 3 and 4, ensuring that they are estimated as accurately as possible.

Sample splitting is employed to separate the data into estimation and inference samples, which helps to avoid overfitting, and hence to achieve valid statistical inference.

The DML framework has gained attention in various domains, including social sciences, computer science, medicine, biostatistics, and economics and finance, because of its ability to address the challenges of causal inference with high-dimensional data. Furthermore, the DML framework has been implemented in both R and Python programming languages as DoubleML (Bach et al., 2021), making it accessible to many users in academic and industry research. In summary, the double machine learning method, as described by Chernozhukov et al. (2018), provides a robust framework for valid statistical inference for tabular data or structured data in structural equation models by integrating high-quality machine learning estimation with sample splitting. Its versatility and applicability across various domains make it a valuable tool for addressing causal inference challenges with complex, high-dimensional controls.

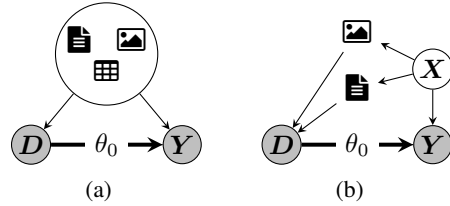


Figure 1: Examples of directed acyclic graphs (DAGs) with image and text confounding. (a) Direct confounding via image, text and tabular data. (b) Treatment decision is driven by text and images. All backdoor paths are blocked by conditioning on both image and text data.

4. Double Machine Learning for Text and Images

In the simplest case, the covariates X are tabular, as discussed in the previous section, and can be represented as $X_{\text{tab}} = (X_1, \dots, X_p)$ such that $X_{\text{tab}} \in \mathbb{R}^p$, $p \in \mathbb{N}$. However, if the controls are unstructured, e.g. in the simple form of RGB images, X can be represented as a tensor such that $X_{\text{img}} \in \mathbb{R}^{3 \times h \times w}$, $h, w \in \mathbb{N}$. For controls in text form, X can be defined as an input representation matrix including the token, segmentation and position embeddings (Devlin et al., 2019) and can therefore be written as $X_{\text{txt}} \in \mathbb{R}^{3 \times S}$, $S \in \mathbb{N}$ where S denotes the sequence length of the input sentence.

If all input modalities are to be used together as controls, X can be represented as a set consisting of $X = (X_{\text{tab}}, X_{\text{txt}}, X_{\text{img}})$ with $X_{\text{tab}} \in \mathbb{R}^p$ for the tabular input, $X_{\text{txt}} \in \mathbb{R}^{3 \times S}$ for the text input and $X_{\text{img}} \in \mathbb{R}^{3 \times h \times w}$ for the image input with $p, h, w, S \in \mathbb{N}$. This results in a high-dimensional input vector, which cannot be directly used for nuisance estimation, but rather can be modeled as input for Deep Learning architectures, resulting in low-dimensional representations. The influence of text and image data is illustrated in Figure 1.

As highlighted in the previous sections, the DML approach relies on high-quality estimates for the nuisance elements $m_0(X)$ and $l_0(X)$, such that the mean squared error (or product of root mean squared errors in Equation 5) converges fast enough. For tabular data these rates are achievable via standard machine learning algorithms such as e.g. lasso (Bickel et al., 2009) or boosting (Luo et al., 2022). Theoretical results on the convergence rates of neural networks are not that clear, due to the large difference in architectures. Among others, see Schmidt-Hieber (2020), Kohler & Langer (2021) or Farrell et al. (2021). These results are mostly geared towards feed forward networks, but highlight that the required theoretical rates are achievable. Nevertheless, more complex neural network architectures as e.g. transformers achieve stunning predictive performance in the respective regression or classification tasks, suggesting

credibly fast convergence and therefore likely fulfilling the conditions for the double machine learning framework.

4.1. Model

To estimate the nuisance functions according to Equations 3 and 4 with the set of multimodal controls X , we need advanced methods. The focus of this work is on multimodal models due to their promising results across different tasks. Utilizing multimodal data fusion is particularly suited for achieving the objective of estimating the causal parameter θ_0 incorporating confounders sourced from tabular features, text and images. Multimodal models are a class of ML models that can effectively handle input data from different modalities such as text, image, video or audio. These models combine information from multiple modalities to improve their predictive power and achieve a better performance compared to individual modalities systems (Rahate et al., 2022). Multimodal data fusion seeks to extract and merge contextual information from multiple modalities in order to enhance decision-making. This is done by taking advantage of the complementary strengths of each modality (Lipkova et al., 2022). Multimodal models can, for example, combine semantic knowledge gained from texts with knowledge of spatial structures obtained from images to learn joint representations of images and texts (Miller et al., 2021). The objective of a multimodal model is to combine features of various modalities (Lee & Rho, 2022). The architecture of these models can be diverse and includes, for example, neural networks capable of processing and analyzing each modality, followed by a fusion module that concatenates the information across modalities (Miller et al., 2021).

4.2. Deep Learning Architecture and Implementation Details

The high-level architecture of our model for the single treatment case is shown in Figure 2. The integration of the modalities occurs through a middle fusion approach, whereby the text and image data are combined at an intermediate representation level, utilizing the embedding output. This hidden state is processed by a linear layer and an activation function. Finally, the embedding $H_E \in \mathbb{R}^E$ provides a E -dimensional representation of the input data that can be used to make predictions or classify the input (Wolf et al., 2020).

We use pre-trained transformer-based models such as BERT (Vaswani et al., 2023) or variants like the robustly optimized BERT Pretraining Approach (RoBERTa) (Liu et al., 2019) or LLMs like Llama (Touvron et al., 2023) for handling the text data. For the image processing, we rely on transformer-based models such as BEIT (Bao et al., 2022) or Vision Transformers (ViTs) (Dosovitskiy et al., 2021). Using models like the SAINT model (Somepalli et al., 2021) for tabular data appears to be satisfactory.

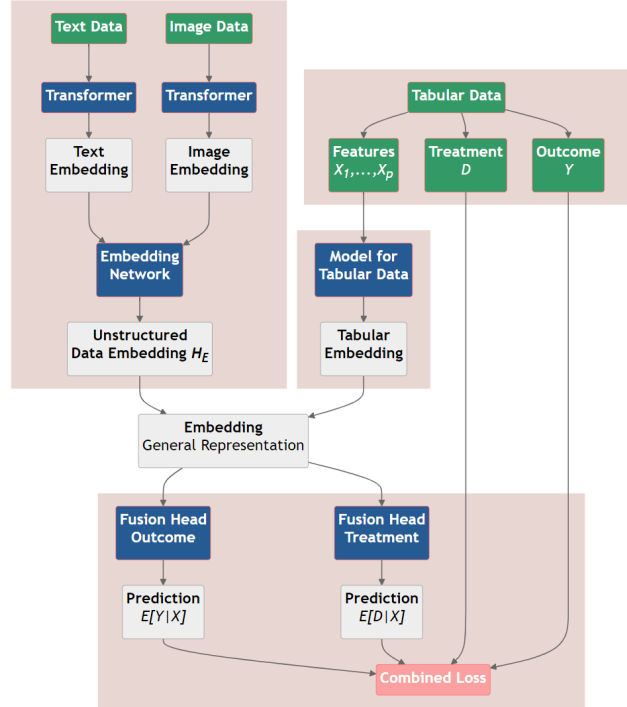


Figure 2: High-Level PLR Model Architecture. Both nuisance components are trained simultaneously with a combined loss.

It is crucial to closely monitor losses of each nuisance component to ensure high-quality predictions:

$$\begin{aligned} \|Y - \hat{l}(X)\|_{P,2} &\leq \|l_0 - \hat{l}(X)\|_{P,2} + \sigma_\epsilon \\ \|D - \hat{m}(X)\|_{P,2} &\leq \|m_0(X) - \hat{m}(X)\|_{P,2} + \sigma_\vartheta. \end{aligned}$$

These considerations contribute to the robustness and effectiveness of the models applied to both unstructured and tabular data, emphasizing the importance of vigilance over nuisance losses. The combined loss function for model training is defined as the product of root mean squared errors:

$$L = \|D - \hat{m}(X)\|_{P_n,2} \|Y - \hat{l}(X)\|_{P_n,2}.$$

Usually the DML framework relies on cross-fitting to ensure the nuisance learners do not overfit. In principle cross-fitting is also possible for neural networks but would increase the computational burden excessively. Instead, we rely on simple sample splitting, such that the neural network is trained on a training set and the estimation of the target parameter θ_0 is performed on a separate test set. Recent simulation results by Bach et al. (2024) suggest that the performance of DML with a single sample split is comparable to a cross-fitting approach in large sample sizes.

5. Simulation Study

The validation of the proposed estimator is a crucial step in ensuring their accuracy and reliability. Unlike predictive

models, the performance of causal models is not straightforward to evaluate in real world applications. The evaluation of causal estimation approaches is generally complicated by the fact that the true causal effect (unlike true labels for predicted outcomes) is not observable, which requires the use of synthetic or semi-synthetic data. In this simulation study, we generate a semi-synthetic dataset with a known treatment effect parameter. We document a generally inherent challenge of simulating multimodal data for causal estimation: Generating credible confounding through unstructured data makes it very hard to uncover the true causal effect parameter. In our data generating process, the confounding operates through labels of the supervised learning tasks such as image classification, which cannot be perfectly predicted by the neural nets. Consequently, a part of the imposed confounding remains unexplained, which prevents exact identification and estimation of the causal parameter. Hence, we consider the true causal parameter as an ideal, but generally infeasible statistical estimate. Our analysis will include simulations to evaluate prediction performance for treatment and outcome, joint loss function values, and variance and bias of the causal effect estimate.

5.1. Simulating Confounding with Text and Images

To evaluate the performance of our model, we generate a semi-synthetic dataset according to the underlying model in Equations 1 and 2

$$\begin{aligned} Y &= \theta_0 D + \tilde{g}_0(\tilde{X}) + \varepsilon, \\ D &= \tilde{m}_0(\tilde{X}) + \vartheta, \end{aligned}$$

where $\tilde{X} = (\tilde{X}_{\text{tab}}, \tilde{X}_{\text{txt}}, \tilde{X}_{\text{img}})$ with the following additive structure

$$\begin{aligned} \tilde{g}_0(\tilde{X}) &= \sum_{\text{mod} \in \{\text{tab}, \text{txt}, \text{img}\}} \tilde{g}_{\text{mod}}(\tilde{X}_{\text{mod}}) \\ \tilde{m}_0(\tilde{X}) &= \sum_{\text{mod} \in \{\text{tab}, \text{txt}, \text{img}\}} \tilde{m}_{\text{mod}}(\tilde{X}_{\text{mod}}) \end{aligned}$$

and $\varepsilon, \vartheta \sim \mathcal{N}(0, 1)$.

Each of the three modality effects is based on a publicly available (simple) non-synthetic dataset which is usually used for classification and regression tasks. All datasets contain one target \tilde{X}_{mod} (outcome or label) and features X_{mod} (image, text etc.). As these datasets have been shown to work well with the respective predictive task, we generate the confounded treatment D and outcome Y based on the targets \tilde{X}_{mod} of the three different datasets instead of the respective features X_{mod} . This ensures a credible confounding, especially for image and text data as the confounding effect depends on content of the image features. Further, the dataset is close to non-synthetic data while still adhering to the partially linear model.

The tabular data is sourced from the DIAMONDS dataset (Wickham, 2016), which includes various attributes of diamonds such as carat, cut, color, clarity, depth, table, price, and measurements (x, y, z). The logarithm of the price column \tilde{X}_{tab} is used to simulate confounding and the other variables will be the tabular input X_{tab} . The tabular data is preprocessed (log-transformation etc.) and downsampled to create a dataset with $N = 50,000$ observations to maintain consistency with the other data modalities of the new semi-synthetic dataset.

The text data component of the semi-synthetic dataset is derived from the IMDB dataset (Maas et al., 2011), which is a collection of movie reviews with corresponding sentiment labels. This dataset is publicly available and has been widely used for sentiment analysis tasks in natural language processing research. The semi-synthetic dataset is based on the training and test sample of the IMDB dataset to match the size of the tabular and image datasets. The binary representation of the sentiment \tilde{X}_{txt} is used to generate confounding while the review constitutes the text input X_{txt} for the set of controls.

The image data component of the semi-synthetic dataset is sourced from the CIFAR-10 dataset (Krizhevsky, 2009), which is a well-known benchmark in the field of computer vision. The CIFAR-10 dataset consists of 60,000 32x32 color images in 10 different classes, with 6,000 images per class. The semi-synthetic dataset is based on the training set, which contains 50,000 images. A numerical representation of the image labels \tilde{X}_{img} is used to obtain a confounding on Y and D while the images will be part of the set of controls as X_{img} .

The effect on the outcome Y is generated via a standardized version of target variable

$$\tilde{g}_{\text{mod}}(\tilde{X}_{\text{mod}}) = \frac{\tilde{X}_{\text{mod}} - \mathbb{E}[\tilde{X}_{\text{mod}}]}{\sigma_{\tilde{X}_{\text{mod}}}}, \quad \text{mod} \in \{\text{tab}, \text{txt}, \text{img}\}$$

to balance the confounding impact of all modalities. Further, the impact on the treatment D is defined via

$$\tilde{m}_{\text{mod}}(\tilde{X}_{\text{mod}}) = -\tilde{g}_{\text{mod}}(\tilde{X}_{\text{mod}}), \quad \text{mod} \in \{\text{tab}, \text{txt}, \text{img}\}$$

to ensure a strong confounding. Due to the negative sign and the additive structure, the confounding effect will ensure that higher outcomes Y occur with lower treatment values D , creating a negative bias. Further, the independence of all three original datasets and the additive negative confounding results in a negative bias even if we only control for a subset of confounding factors.

The treatment effect is set to $\theta_0 = 0.5$ and both $\tilde{g}_0(X)$ and $\tilde{m}_0(X)$ are rescaled to ensure a signal-to-noise ratio of 2 for Y and D (given unit variances of the error terms).

A generally inherent challenge of this type of data generating processes is the dependency on the target of the

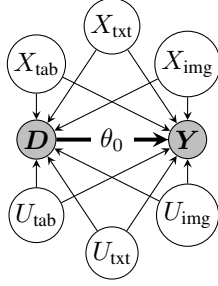


Figure 3: DAG for the semi-synthetic dataset. The confounding via the features $X = (X_{\text{tab}}, X_{\text{txt}}, X_{\text{img}})$ can be adjusted for, whereas the unexplained/noise parts $U = (U_{\text{tab}}, U_{\text{txt}}, U_{\text{img}})$ are unobserved.

modality \tilde{X}_{mod} , which might not be fully explained by the corresponding features X_{mod} . For example, the price of the DIAMONDS dataset can not be perfectly predicted, introducing a small part of confounding which can not be controlled for by using the tabular features X_{tab} instead of \tilde{X}_{tab} (logarithm of price), as shown in the DAG in Figure 3. Consequently, the estimate $\hat{\theta}$ might only be able to account for the part of confounding which can be explained by the input features as

$$\tilde{X}_{\text{mod}} = \mathbb{E}[\tilde{X}_{\text{mod}} | X_{\text{mod}}] + U_{\text{mod}},$$

where U_{mod} can not be controlled for. Nevertheless, since all modalities contribute a negative bias, the semi-synthetic dataset can be used as a benchmark with an oracle upper bound of an effect estimate of $\theta_0 = 0.5$. To evaluate the confounding one can evaluate a basic ordinary least squares model with outcome Y on the treatment variable D (excluding all confounding variables). The resulting effect estimate

$$\hat{\theta}_{\text{OLS}} = -0.4594,$$

can be interpreted as a lower bound for the effect estimate. Accordingly, all evaluated models should estimate the parameter between -0.4594 and 0.5 , where higher values indicate better bias correction (ignoring sampling uncertainty).

To further access the predictive performance of the nuisance models, we can rely on oracle predictions of

$$\begin{aligned} \tilde{m}_0(\tilde{X}) &:= \mathbb{E}[D | \tilde{X}] \\ \tilde{l}_0(\tilde{X}) &:= \mathbb{E}[Y | \tilde{X}] = \theta_0 \tilde{m}_0(\tilde{X}) + \tilde{g}_0(\tilde{X}). \end{aligned}$$

Evaluating the oracle predictions $\tilde{m}_0(\tilde{X})$ and $\tilde{l}_0(\tilde{X})$ results in the following upper bounds for the performance of the nuisance estimators

$$\begin{aligned} R^2(D, \tilde{m}_0(\tilde{X})) &= 0.6713 \\ R^2(Y, \tilde{l}_0(\tilde{X})) &= 0.5845 \end{aligned}$$

on the whole dataset of $N = 50,000$ observations, which is to be expected due to the choice of signal-to-noise ratio. Again, since models only have access to the features $X = (X_{\text{tab}}, X_{\text{txt}}, X_{\text{img}})$ instead of the targets $\tilde{X} =$

$(\tilde{X}_{\text{tab}}, \tilde{X}_{\text{txt}}, \tilde{X}_{\text{img}})$, the above values represent lower and upper bounds for R^2 .

5.2. Results

In this section, two different estimation approaches based on the proposed architecture are evaluated on the semi-synthetic dataset and compared to a baseline model. To ensure that all models are comparable and only differ correction for confounding, we rely on the implementation of the partially linear regression model from the DoubleML package (Bach et al., 2022). All models only differ in the nuisance estimates, which are passed to the DoubleML implementation.

The *Baseline Model* is a standard DML approach, relying only on tabular data. The estimation of the nuisance elements is based on the LightGBM package (Ke et al., 2017) only using the features X_{tab} . Due to the construction of the semi-synthetic data, the resulting estimate should be highly biased, as the model is only able to account for the part of the confounding, which is generated via the tabular data.

The *Deep Model* relies on the proposed architecture in Figure 2 and uses the out-of-sample predictions of $\hat{m}(X)$ and $\hat{l}(X)$ generated from the model. As the model utilizes multi-modal features $X = (X_{\text{tab}}, X_{\text{txt}}, X_{\text{img}})$, the estimate should be much less biased than the Baseline Model. For our simulation study, we use the RoBERTa Model pretrained on a Twitter Dataset (Loureiro et al., 2022) as the text model. For the image processing we rely on a ViT Model pretrained on the ImageNet-21k Dataset (Wightman, 2019). Both models are implemented in the Hugging Face transformers package (Wolf et al., 2020). The tabular data is handled by a SAINT model (Somepalli et al., 2021) implemented in the pytorch-widedeep package (Zaurin & Mulinka, 2023).

The *Embedding Model* also relies on the proposed architecture in Figure 2, but does not use the generated predictions directly. Instead the generated embedding H_E is used together with the tabular features X_{tab} as input for a boosting algorithm. Since neural networks are often outperformed by tree based models, such as gradient boosted trees, on tabular data (Grinsztajn et al., 2022), the model might perform better on the tabular part of the data, while still accounting for the information contained in the image and text components.

In order to compare the predictive performance of the models, a relative r^2 -score with respect to the upper bound as described in Section 5.1 is defined as

$$\begin{aligned} 0 \leq r^2(D, \hat{m}) &:= \frac{R^2(D, \hat{m}(X))}{R^2(D, \tilde{m}_0(\tilde{X}))} \leq 1 \\ 0 \leq r^2(Y, \hat{l}) &:= \frac{R^2(Y, \hat{l}(X))}{R^2(Y, \tilde{l}_0(\tilde{X}))} \leq 1 \end{aligned}$$

The results of the Baseline Model, Embedding Model and

Table 1: Results of Simulation Study. Reported: mean \pm sd. over five random train-test splits.

	Baseline	Embedding	Deep
$r^2(Y, \hat{l}_0)$	0.27 ± 0.02	0.88 ± 0.02	0.90 ± 0.02
$r^2(D, \hat{m}_0)$	0.29 ± 0.01	0.89 ± 0.01	0.90 ± 0.01
$\hat{\theta}$	-0.32 ± 0.01	0.28 ± 0.01	0.28 ± 0.01

Higher = better (best in bold)

Deep Model are presented in Table 1 with the r^2 -score values for the confounding functions \hat{l} and \hat{m} as well as the estimated treatment effect $\hat{\theta}$. Notably, the confounding effect is substantial and designed to create a negative bias, wherein higher outcomes Y are associated with lower treatment values D . This configuration enables a comprehensive evaluation of bias correction methods, particularly in scenarios where traditional approaches may struggle to account for confounding adequately.

The results presented in Table 1 demonstrate the tangible impact of incorporating multimodal information into the estimation process. The Baseline Model, which relies solely on tabular data, exhibits significant bias in estimating the treatment effect ($\hat{\theta} = -0.32 \pm 0.01$), indicative of insufficient control over confounding factors originating from text and image modalities. Figure 4 shows the boxplots of the r^2 -scores of all three models. This comparative analysis of r^2 -scores highlights the great predictive performance of the Embedding and Deep Model (approximately 90% of predictable variance), indicating its ability to utilize both structured and unstructured data for more accurate estimation of treatment effects.

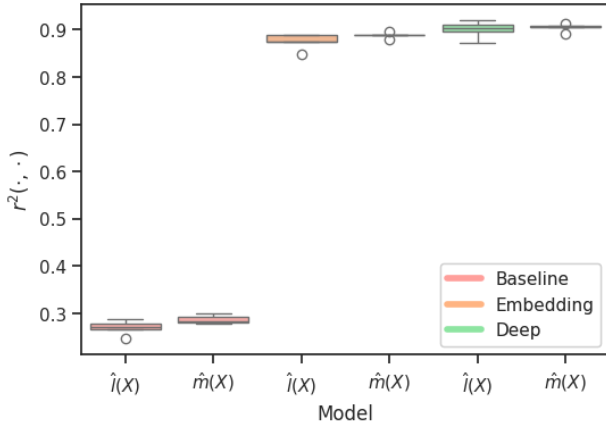
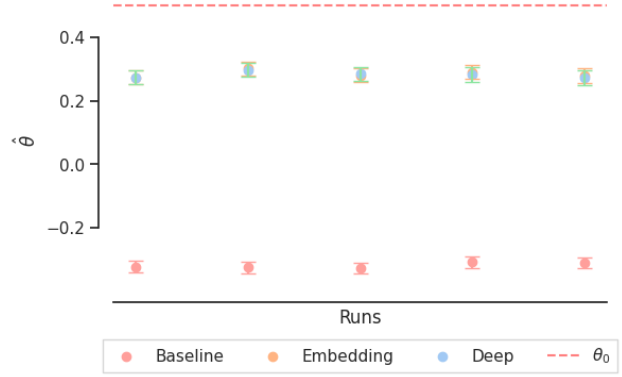
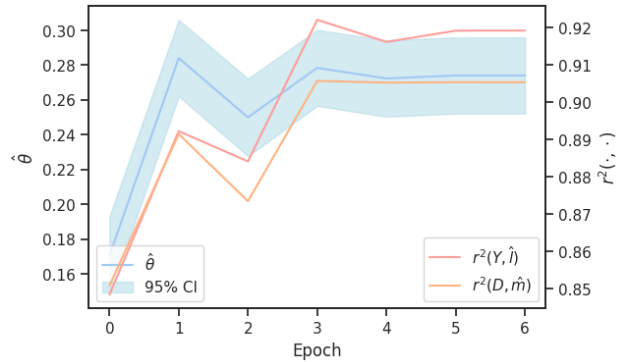

 Figure 4: Boxplots of r^2 -Scores. As anticipated, the tabular data provides only 30% explanatory power, but the inclusion of unstructured data increases the predictable variance to approximately 90%.

 Figure 5 shows boxplots of the estimated $\hat{\theta}$ values including the 95% confidence interval.

 Figure 5: Boxplots of $\hat{\theta}$. The Embedding Model and Deep Model have similar estimates. This indicates a stable and information-rich embedding H_E , which provides a high explanatory contribution independent of the subsequent ML method for predicting Y and D (Bengio et al., 2014). θ_0 represents the upper bound.

The Deep Model is able to give a continuous estimation of θ_0 after each training epoch, which is shown in Figure 6 including the 95% confidence interval as well. As can be seen, the estimation $\hat{\theta}$ gets closer to the true value θ_0 during the training process. The observed trends in the r^2 -scores ($r^2(Y, \hat{l})$ and $r^2(D, \hat{m})$) and in the coefficient estimate ($\hat{\theta}$) provide valuable insights into the relationship between the prediction performance and the bias correction of the causal estimate.


 Figure 6: Continuous estimation of θ_0 . Both, the r^2 -scores and the coefficient estimates gradually converge to stable values over the epochs.

6. Conclusion

In this article we extend the double machine learning framework to allow for tabular data, text, and images as confounding variables. This makes it possible to provide valid inference of the causal target parameter in this setting. Given the increasing availability of multimodal data, we consider our paper as an important innovation in the field of causal machine learning. Incorporating information from images

or text can help to improve results from causal studies, either by capturing otherwise unmeasured confounding or by improving the precision of statistical estimators. To validate our approach, we set up a new framework to generate semi-synthetic data with multimodal data that addresses inherent challenges in this type of simulation studies. The proposed method might be of independent interest to the scientific community. Our semi-synthetic numerical experiments demonstrated the model’s ability to incorporate the confounding that is contained in the text and image data. The performance substantially improved as compared to a benchmark model that does not account for this information. We acknowledge that in our simulations our model does not consistently estimate the true causal parameter. This, however, is rather the consequence of the inherent limitations to simulated text and image data for causal analysis rather than a shortcoming of our neural network architecture, that is based on state-of-the-art approaches. To the best of our knowledge, we are not aware of any other approach to handle multimodal data for causal inference. Our approach was tailored to the partially linear regression model but is generally applicable to any kind of causal model that fits in the double machine learning framework, for example non-parametric models to estimate treatment effects or causal models that explicitly address variation over time, such as panel data or difference-in-differences models. In these cases, the architecture of our neural network would have to be adjusted to the definitions of the nuisance components in these models. Moreover, our approach could also be extended to other kinds of unstructured data, like graphs, networks, audio or video data.

Impact Statement

This paper presents work whose goal is to advance the fields of Machine Learning and Causal Inference. There are many potential societal consequences of our work, none of which we feel must be specifically highlighted here.

References

- Bach, P., Chernozhukov, V., Kurz, M. S., and Spindler, M. Doubleml – an object-oriented implementation of double machine learning in R. 2021. doi: 10.48550/arxiv.2103.09603.
- Bach, P., Chernozhukov, V., Kurz, M. S., and Spindler, M. Doubleml: an object-oriented implementation of double machine learning in Python. *The Journal of Machine Learning Research*, 23(1):2469–2474, 2022.
- Bach, P., Schacht, O., Chernozhukov, V., Klaassen, S., and Spindler, M. Hyperparameter tuning for causal inference with double machine learning: A simulation study. In *3rd Causal Learning and Reasoning*, 2024. URL <https://openreview.net/forum?id=h0ecxkungr>.
- Bao, H., Dong, L., Piao, S., and Wei, F. Beit: Bert pre-training of image transformers, 2022.
- Bengio, Y., Courville, A., and Vincent, P. Representation learning: A review and new perspectives, 2014.
- Bickel, P. J., Ritov, Y., and Tsybakov, A. B. Simultaneous analysis of Lasso and Dantzig selector. *The Annals of Statistics*, 37(4):1705 – 1732, 2009. doi: 10.1214/08-AOS620. URL <https://doi.org/10.1214/08-AOS620>.
- Chan, A. J., Chien, I., Moseley, E. T., Salman, S., Bourland, S. K., Lamas, D., Walling, A. M., and Tulskey, J. A. Deep learning algorithms to identify documentation of serious illness conversations during intensive care unit admissions. *Palliative Medicine*, 2018. doi: 10.1177/0269216318810421.
- Chernozhukov, V., Chetverikov, D., Demirer, M., Duflo, E., Hansen, C., Newey, W., and Robins, J. Double/debiased machine learning for treatment and structural parameters. *The Econometrics Journal*, 21(1):C1–C68, 01 2018. ISSN 1368-4221. doi: 10.1111/ectj.12097. URL <https://doi.org/10.1111/ectj.12097>.
- Devlin, J., Chang, M.-W., Lee, K., and Toutanova, K. Bert: Pre-training of deep bidirectional transformers for language understanding, 2019.
- Dosovitskiy, A., Beyer, L., Kolesnikov, A., Weissenborn, D., Zhai, X., Unterthiner, T., Dehghani, M., Minderer, M., Heigold, G., Gelly, S., Uszkoreit, J., and Houshy, N. An image is worth 16x16 words: Transformers for image recognition at scale, 2021.
- Egami, N., Fong, C. J., Grimmer, J., Roberts, M. E., and Stewart, B. M. How to make causal inferences using texts, 2018.
- Farrell, M. H., Liang, T., and Misra, S. Deep neural networks for estimation and inference. *Econometrica*, 89(1): 181–213, 2021.
- Feder, A., Keith, K. A., Manzoor, E., Pryzant, R., Sridhar, D., Wood-Doughty, Z., Eisenstein, J., Grimmer, J., Reichart, R., Roberts, M. E., Stewart, B. M., Veitch, V., and Yang, D. Causal inference in natural language processing: Estimation, prediction, interpretation and beyond. *Transactions of the Association for Computational Linguistics*, 10:1138–1158, 2022. doi: 10.1162/tacl.a.00511. URL <https://aclanthology.org/2022.tacl-1.66>.

- Foster, D. J. and Syrgkanis, V. Orthogonal statistical learning. *The Annals of Statistics*, 51(3):879 – 908, 2023. doi: 10.1214/23-AOS2258. URL <https://doi.org/10.1214/23-AOS2258>.
- Goodfellow, I., Bengio, Y., and Courville, A. *Deep Learning*. MIT Press, 2016. <http://www.deeplearningbook.org>.
- Grinsztajn, L., Oyallon, E., and Varoquaux, G. Why do tree-based models still outperform deep learning on tabular data?, 2022.
- Härdle, W., Müller, M., Sperlich, S., and Werwatz, A. *Nonparametric and Semiparametric Models*. Springer Series in Statistics. Springer Berlin Heidelberg, 2012. ISBN 9783642171468. URL <https://books.google.de/books?id=wqX7CAAQBAJ>.
- Jerzak, C. T., Johansson, F., and Daoud, A. Estimating causal effects under image confounding bias with an application to poverty in africa, 2023a.
- Jerzak, C. T., Johansson, F., and Daoud, A. Image-based treatment effect heterogeneity, 2023b.
- Jerzak, C. T., Johansson, F., and Daoud, A. Integrating earth observation data into causal inference: Challenges and opportunities, 2023c.
- Ke, G., Meng, Q., Finley, T., Wang, T., Chen, W., Ma, W., Ye, Q., and Liu, T.-Y. Lightgbm: A highly efficient gradient boosting decision tree. In Guyon, I., Luxburg, U. V., Bengio, S., Wallach, H., Fergus, R., Vishwanathan, S., and Garnett, R. (eds.), *Advances in Neural Information Processing Systems*, volume 30. Curran Associates, Inc., 2017. URL https://proceedings.neurips.cc/paper_files/paper/2017/file/6449f44a102fde848669bdd9eb6b76fa-Paper.pdf.
- Kohler, M. and Langer, S. On the rate of convergence of fully connected deep neural network regression estimates. *The Annals of Statistics*, 49(4):2231–2249, 2021.
- Krizhevsky, A. Learning multiple layers of features from tiny images. Technical report, 2009.
- Lee, S. and Rho, M. Multimodal deep learning applied to classify healthy and disease states of human microbiome. 12, 2022. doi: 10.1038/s41598-022-04773-3.
- Lipkova, J., Chen, R. J., Chen, B., Lu, M. Y., Barbieri, M., Shao, D., Vaidya, A. J., Chen, C., Zhuang, L., Williamson, D. F. K., Shaban, M., Chen, T. Y., and Mahmood, F. Artificial intelligence for multi-modal data integration in oncology. 40(10):1095–1110, 2022. ISSN 1535-6108. doi: 10.1016/j.jco.2022.09.012. URL <https://www.sciencedirect.com/science/article/pii/S153561082200441X>.
- Liu, Y., Ott, M., Goyal, N., Du, J., Joshi, M., Chen, D., Levy, O., Lewis, M., Zettlemoyer, L., and Stoyanov, V. Roberta: A robustly optimized bert pretraining approach, 2019.
- Loureiro, D., Barbieri, F., Neves, L., Anke, L. E., and Camacho-Collados, J. Timelms: Diachronic language models from twitter, 2022.
- Luo, Y., Spindler, M., and Kück, J. High-dimensional l_2 boosting: Rate of convergence, 2022.
- Maas, A. L., Daly, R. E., Pham, P. T., Huang, D., Ng, A. Y., and Potts, C. Learning word vectors for sentiment analysis. In *Proceedings of the 49th Annual Meeting of the Association for Computational Linguistics: Human Language Technologies*, pp. 142–150, Portland, Oregon, USA, June 2011. Association for Computational Linguistics. URL <http://www.aclweb.org/anthology/P11-1015>.
- Masukawa, K., Aoyama, M., Yokota, S., Nakamura, J., Ishida, R., and Nakayama, M. Machine learning models to detect social distress, spiritual pain, and severe physical psychological symptoms in terminally ill patients with cancer from unstructured text data in electronic medical records. *Palliative Medicine*, 2022. doi: 10.1177/02692163221105595.
- Melnychuk, V., Frauen, D., and Feuerriegel, S. Causal transformer for estimating counterfactual outcomes, 2022.
- Miller, S., Howard, J., Adams, P., Schwan, M., and Slater, R. Multi-modal classification using images and text. 3(3), 2021. URL <https://scholar.smu.edu/datasciencereview/vol3/iss3/6>.
- Rahate, A., Walambe, R., Ramanna, S., and Kotecha, K. Multimodal co-learning: Challenges, applications with datasets, recent advances and future directions. 81:203–239, 2022. ISSN 15662535. doi: 10.1016/j.inffus.2021.12.003. URL <http://arxiv.org/abs/2107.13782>.
- Schmidt-Hieber, J. Nonparametric regression using deep neural networks with relu activation function. 2020.
- Somepalli, G., Goldblum, M., Schwarzschild, A., Bruss, C. B., and Goldstein, T. Saint: Improved neural networks for tabular data via row attention and contrastive pre-training, 2021.
- Sridhar, D. and Blei, D. M. Causal inference from text: A commentary. *Science Advances*, 8(42): eade6585, 2022. doi: 10.1126/sciadv.ade6585. URL

- <https://www.science.org/doi/abs/10.1126/sciadv.ade6585>.
- Touvron, H., Lavril, T., Izacard, G., Martinet, X., Lachaux, M.-A., Lacroix, T., Rozière, B., Goyal, N., Hambro, E., Azhar, F., Rodriguez, A., Joulin, A., Grave, E., and Lample, G. Llama: Open and efficient foundation language models, 2023.
- Vaswani, A., Shazeer, N., Parmar, N., Uszkoreit, J., Jones, L., Gomez, A. N., Kaiser, L., and Polosukhin, I. Attention is all you need, 2023.
- Veitch, V., Sridhar, D., and Blei, D. Adapting text embeddings for causal inference. In Peters, J. and Sontag, D. (eds.), Proceedings of the 36th Conference on Uncertainty in Artificial Intelligence (UAI), volume 124 of Proceedings of Machine Learning Research, pp. 919–928. PMLR, 03–06 Aug 2020. URL <https://proceedings.mlr.press/v124/veitch20a.html>.
- Wickham, H. ggplot2: Elegant Graphics for Data Analysis. Springer-Verlag New York, 2016. ISBN 978-3-319-24277-4. URL <https://ggplot2.tidyverse.org>.
- Wightman, R. Pytorch image models. <https://github.com/rwightman/pytorch-image-models>, 2019.
- Wolf, T., Debut, L., Sanh, V., Chaumond, J., Delangue, C., Moi, A., Cistac, P., Rault, T., Louf, R., Funtowicz, M., Davison, J., Shleifer, S., von Platen, P., Ma, C., Jernite, Y., Plu, J., Xu, C., Scao, T. L., Gugger, S., Drame, M., Lhoest, Q., and Rush, A. M. Transformers: State-of-the-art natural language processing. In Proceedings of the 2020 Conference on Empirical Methods in Natural Language Processing: System Demonstrations, pp. 38–45, Online, October 2020. Association for Computational Linguistics. URL <https://www.aclweb.org/anthology/2020.emnlp-demos.6>.
- Wu, Z., Duan, X., and Zhang, W. Bayesian analysis of tweedie compound poisson partial linear mixed models with nonignorable missing response and covariates. Entropy, 2023. doi: 10.3390/e25030506.
- Zaurin, J. R. and Mulinka, P. pytorch-widedeep: A flexible package for multimodal deep learning. Journal of Open Source Software, 8(86):5027, June 2023. doi: 10.21105/joss.05027. URL <https://joss.theoj.org/papers/10.21105/joss.05027>.
- Zhang, A., Lipton, Z. C., Li, M., and Smola, A. J. Dive into Deep Learning. Cambridge University Press, 2023. <https://D2L.ai>.
- Zhang, D., Yin, C., Zeng, J., Yuan, X., and Zhang, P. Combining structured and unstructured data for predictive models: A deep learning approach. BMC Medical Informatics and Decision Making, 2020. doi: 10.1186/s12911-020-01297-6.

A. Appendix

A.1. Definitions

Let V be a random variable and V_1, \dots, V_n iid. realizations of V .

Define

$$\mathbb{E}_n[V] := \frac{1}{n} \sum_{i=1}^n V_i$$

and the correspondingly

$$\begin{aligned} \|V\|_{P,2} &:= \mathbb{E}[V^2] \\ \|V\|_{P_n,2} &:= \mathbb{E}_n[V^2]. \end{aligned}$$

Further, define

$$R^2(V, \hat{V}) = 1 - \frac{\sum_{i=1}^n (V_i - \hat{V}_i)^2}{\sum_{i=1}^n (V_i - \mathbb{E}_n[V])^2}.$$

for two random variables V and \hat{V} .

A.2. Semi-Synthetic Dataset

This subsection includes further information regarding the semi-synthetic dataset. Due to the distribution of the noise and centering of the confounding components it should hold

$$\begin{aligned} \mathbb{E}[Y] &= \mathbb{E}[D] = 0 \\ \text{Var}(Y) &= \text{Var}(D) = 3. \end{aligned}$$

Descriptives regarding the treatment and outcome variable.

	Y	D
count	50000	50000
mean	0.006948	-0.000755
std	1.734030	1.738060
min	-6.233601	-6.461094
25%-quantile	-1.184978	-1.208271
50%-quantile	0.014107	-0.000240
75%-quantile	1.190921	1.193110
max	6.169482	6.260997

The oracle root mean squared errors for the nuisance components are

$$\begin{aligned} \|D - \tilde{m}_0(\tilde{X})\|_{P_n,2} &= 0.9965 \\ \|Y - \tilde{l}_0(\tilde{X})\|_{P_n,2} &= 1.1177. \end{aligned}$$